Check for updates

Enhanced electroreduction of CO_2 to ethanol *via* enriched intermediates at high CO_2 pressures†

Rongxing Qiu,[a] Jun Jia, [ID] [a] Li Peng, [ID] *[a] Ruiqing Li,[a] Sen Yan, [ID] [a] Jiaran Li,[a] Jie Zhang,[b] Daniel T. Sun,[c,d] Zhipeng Lan,[a] Tianwei Xue,[a] Guangkuo Xu,[a] Linxiao Cui,[a] Zeyu Lv,[a] Cheng Li,[a] Yanzhen Hong,[a] Yuzheng Guo, [ID] [e] Bin Ren, [ID] [a] Shuliang Yang,*[f] Jun Li [ID] *[a] and Buxing Han [ID] [g]

Electrochemical conversion of CO_2 into liquid fuels such as ethanol, powered by renewable electricity, is an efficient strategy for CO_2 utilization to produce high value-added products. In this work, we discovered that the primary C_{2+} product could be switched from gaseous ethylene to liquid ethanol by directly increasing the CO_2 pressure when $Cu_2O@Cu$ with a hollow sphere morphology was adopted as the catalyst. The faradaic efficiency (FE) of ethanol reached as high as 36.6% at a low overpotential of −1.0 V *vs.* Ag/AgCl (−0.48 V *vs.* RHE) at 100 bar, which was 4.6 times higher than that of 1 bar. Moreover, faster kinetics and lower overpotential for ethanol formation were obtained at high CO_2 pressures. *In situ* Raman spectroscopy studies at different pressures in combination with density functional theory calculations demonstrated that the *CO surface coverage was increased significantly at increased CO_2 pressure, which is responsible for facilitating ethanol formation during the electrochemical CO_2RR. This study provides a novel and promising strategy for the selective production of ethanol on Cu-based catalysts by facilely adjusting the CO_2 pressure.

Introduction

Carbon capture and conversion has received considerable attention as a potential means of reducing anthropogenic CO_2 emissions.[1] The electrochemical CO_2 reduction reaction (CO_2RR) into high value-added chemicals and fuels has great potential for closing the carbon cycle and alleviating the energy shortage crisis.[2,3] Tremendous effort has been devoted to developing a series of novel heterogeneous catalysts for the electrochemical conversion of CO_2 into C_1 products (*i.e.*, $CO^{[4–7]}$

and $HCOO^{−\,[8,9]}$) using renewable energy. However, further reduction of these chemicals into more valuable chemicals and fuels (C_{2+} compounds, *i.e.*, ethylene,[10–13] ethanol[14–18] and *n*-propanol[19,20]) is highly desired. Ethylene and ethanol, as vital C_{2+} chemicals with high energy density, share many intermediates in the 12-electron transfer process. Obtaining ethanol from electrochemical CO_2 reduction is an extremely attractive approach owing to its high energy density and economic value. However, there are still numerous challenges that exist in selectively producing ethanol due to the C–C coupling limitation and the presence of the competitive reaction for ethylene.[21,22]

At present, Cu-based materials have been regarded as the most effective catalysts to generate C_{2+} products by the electroreduction of CO_2.[23,24] Many tactics for designing catalysts have been applied to CO_2 (CO) electroreduction to generate C_{2+} products, including oxide-derived copper,[25–27] selective facet exposure,[28–30] morphological control,[31,32] heteroatom doping/bimetallic strategies,[33–35] vacancy effect,[36] molecular modifications,[15,37,38] introducing compressive strain,[39] and free-copper based catalysts.[40,41] Other experimental parameters including local pH environment,[42] temperature[43] and pressure[44,45] have also been considered, which would greatly affect the selectivity of products in the CO_2RR.

It has been recognized that the low solubility of CO_2 in the aqueous electrolyte at ambient pressure often forms limited

[a] College of Chemistry and Chemical Engineering, Xiamen University, Xiamen 361005, Fujian, PR China. E-mail: li.peng@xmu.edu.cn, junnyxm@xmu.edu.cn
[b] Department of Chemistry, National University of Singapore, 3 Science Drive 3, 117543, Singapore
[c] Sunchem LLC, 395 South Van Ness Ave., San Francisco, CA 94103, USA
[d] The Molecular Foundry, Lawrence Berkeley National Laboratory, 1 Cyclotron Road, Berkeley, California 94720, USA
[e] The Institute of Technological Sciences, Wuhan University, Wuhan 430072, Hubei, PR China
[f] College of Energy, Xiamen University, Xiamen 361102, Fujian, PR China. E-mail: ysl@xmu.edu.cn
[g] Beijing National Laboratory for Molecular Sciences, CAS Key Laboratory of Colloid and Interface and Thermodynamics, CAS Research/Education Center for Excellence in Molecular Sciences, Institute of Chemistry, Chinese Academy of Sciences, Beijing 100190, PR China

†Electronic supplementary information (ESI) available. See DOI: https://doi.org/10.1039/d2gc03343g

active carbon species, which results in lower current density and inferior selectivity.[46,47] Thus, adjusting the type of electrolyte is a prevalent approach to improve CO_2 solubility such as using ionic liquid-based electrolytes.[48–50] Furthermore, some research groups have reported that increasing the CO_2 concentration by increasing CO_2 pressure can effectively accelerate mass transfer and thus enhance the current density, along with suppressing the hydrogen evolution reaction (HER) to improve CO_2RR selectivity.[51,52] For example, Fontecave *et al.* have reported that an Ag alloyed Zn electrode can drastically increase the partial current density of CO production from -21 mA cm^{-2} at 1 bar to -286 mA cm^{-2} at 9.5 bar. Meanwhile, FE_{CO} maintained an average of 90% over 40 h and an average of 85% over 100 h at 9.5 bar.[53] Dai *et al.* have reported that square-wave-Cu_2O/Cu can reduce CO_2 electrochemically to nearly pure formate at 45 bar, while the HER was the dominant reaction at ambient pressure.[46] Typically, C_1 chemicals are the primary products in the electrochemical CO_2RR at high pressures in previous studies. However, there are very rare studies realizing CO_2–ethanol conversion using electrical energy at high pressures especially above the supercritical pressure as far as we know, which highly deserves further exploration.

Herein, a Cu_2O@Cu hollow sphere catalyst (denoted as HS-Cu) was prepared successfully and its performance for CO_2 electrocatalysis at different CO_2 pressures was studied comprehensively. We surprisingly discovered that the product distribution could be regulated remarkably with an increase in the CO_2 pressure, accompanied by increasing the current density. In particular, at ambient pressure, a broad distribution of products (H_2, CO, CH_4, HCOOH, C_2H_4, CH_3CH_2OH and *n*-propanol) was observed, and ethylene was the main C_{2+} product. Interestingly, ethylene production was suppressed and the production of ethanol was improved greatly by increasing the CO_2 pressure. The FE of ethanol could reach as high as 36.6% at a low overpotential of -1.0 V *vs.* Ag/AgCl (-0.48 V *vs.* RHE) at 100 bar, which was 4.6 times higher than that of 1 bar. Moreover, *in situ* Raman spectroscopy measurements at different CO_2 pressures coupled with density-functional theory (DFT) calculation studies demonstrate that denser *CO surface coverage at a higher CO_2 pressure is responsible for the promotion of ethanol formation during the CO_2 electrocatalysis process. To the best of our knowledge, this is the first report using a Cu catalyst to mainly produce liquid ethanol from the CO_2RR only with the assistance of a high CO_2 pressure. The primary CO_2RR products could be easily switched from gaseous ethylene at ambient pressure into liquid ethanol at a high CO_2 pressure.

Experimental

Materials and chemicals

Copper(II) chloride dihydrate ($CuCl_2 \cdot 2H_2O$, AR), sodium hydroxide (NaOH, AR), D-glucose (AR), potassium bicarbonate (AR), dimethyl sulfoxide (DMSO, AR) and isopropanol

(AR) were produced by Sinopharm Chemical Reagent Co., Ltd. Deuterium oxide (D_2O, 99.9 atom% D) was provided by Energy Chemical. Nafion solution (5 wt% in water and isopropanol) was obtained from Meryer (Shanghai) Chemical Technology Co., Ltd. Conductive carbon paper (hydrophobic) was purchased from Suzhou Sinero Technology Co., Ltd. CO_2 (99.999%) was provided by Fuzhou Xinhang Industrial Gases Co., Ltd. Unless otherwise noted, deionized water (18 MΩ cm^{-2}) was used throughout this work.

Catalyst preparation

The Cu_2O@Cu hollow sphere catalyst was prepared according to the reported literature with some modifications.[54] $CuCl_2 \cdot 2H_2O$ (0.3410 g) was added to a mixed solution of 20 mL of ethylene glycol and 10 mL of deionized water, and the solution was stirred for 10 min and transferred into a 100 mL two-necked flask immersed in a 60 °C water bath. Whereafter, 10 mL of NaOH (2 g) aqueous solution was added drop by drop. After 5 min, 10 mL of D-glucose (2 g) solution was added rapidly and kept at 60 °C for 30 min. The resulting product was centrifuged, and rinsed with distilled water several times. Finally, the Cu_2O@Cu hollow sphere catalyst was obtained by drying it in a vacuum oven at 70 °C for 12 h.

Characterization of materials

Powder XRD was recorded using a Rigaku SmartLab-SE powder X-ray diffractometer with Cu Kα radiation (λ = 1.5418 Å) at room temperature. SEM images were acquired using a field emission scanning electron microscope from ZEISS Sigma. The morphology of the products was measured using an FEI Tecnai F30 transmission electron microscope at an acceleration voltage of 300 kV. XPS measurements were implemented with a Thermo Escalab 250Xi spectrometer using a photon energy of 461 eV at an energy resolution of 0.1 eV. ^{1}H NMR spectra were operated using a Bruker AVANCE III 500 MHz nuclear magnetic resonance spectrometer. *In situ* Raman measurements were conducted with a Renishaw invia instrument using a 633 nm excitation laser and signals were recorded using 20 s integration in a home-made high pressure *in situ* Raman cell setup with a three-electrode, the laser power was 0.4 mW, and the objective (Nikon, ×10, NA 0.25) was used for exciting and collecting the Raman signals.

Preparation of the working electrode

The as-prepared Cu_2O@Cu hollow sphere catalyst (10 mg) was dispersed in 1980 μL of isopropanol and 20 μL of Nafion solution (5 wt% in water and isopropanol), followed by ultrasonication for 1 h at room temperature. Then 200 μL of catalyst ink was drop-coated onto hydrophobic carbon paper (geometric area: 1 × 1 cm^2), the catalyst loading was about 1 mg cm^{-2}, and the electrode was dried in a vacuum oven at 70 °C for 12 h. HS-Cu was then obtained by *in situ* electroreduction of the Cu_2O@Cu hollow sphere catalyst.

Results and discussion

The HS-Cu catalyst was first synthesized through a simple wet-chemical method. Scanning electron microscopy (SEM) and transmission electron microscopy (TEM) images of the $Cu_2O@Cu$ catalyst exhibited a hollow sphere morphology (Fig. 1a and b). High-resolution TEM (HR-TEM) images (Fig. 1c) revealed that the two different sets of lattice fringes in $Cu_2O@Cu$ correspond to the (111) facet of Cu_2O and the (111) facet of Cu, respectively. The X-ray diffraction (XRD) pattern (Fig. 1d) showed three peaks located at 43.4°, 50.5° and 74.1°, corresponding to the diffraction from the Cu(111), (200) and (220) facets, respectively. Furthermore, the peak at 36.6° could be assigned to the diffraction from the $Cu_2O(111)$ facet, which was consistent with the HR-TEM characterization results. Two peaks at 953.8 eV and 933.9 eV were observed in the Cu 2p X-ray photoelectron spectroscopy (XPS) spectra (Fig. 1e), corresponding to Cu^{2+}, which could be caused by the rapid and unavoidable surface oxidation of Cu^+/Cu^0 when exposed to the air.[55,56] Auger electron spectroscopy (AES) of Cu LMM showed two peaks located at 574.1 eV and 569.2 eV, corresponding to Cu^+ and Cu^0, respectively (Fig. 1f). Taken together, the HS-Cu catalyst containing Cu^+ and Cu^0 was synthesized successfully.

HS-Cu was then obtained by *in situ* electroreduction of the $Cu_2O@Cu$ hollow sphere catalyst *via* five runs of linear sweep voltammetry (LSV) with a scan speed of 20 mV s^{-1} over a potential range from −0.3 V to −2.1 V *vs.* Ag/AgCl. The XRD pattern of HS-Cu displayed only metallic Cu facets (Cu(111),

Cu(200) and Cu(220)) as shown in Fig. S1.† Whereafter, the CO_2RR performance over HS-Cu at ambient and high pressure was inspected carefully. For the electrochemical measurement at ambient and high CO_2 pressures, the CO_2 electroreduction reaction was performed in a high-pressure electrolytic cell with a two-compartment PEEK lining separated by a proton exchange membrane to prevent the crossover of liquid products (Fig. 2a and Fig. S2†). The concentration of active CO_2 (aq.) and H_2CO_3 species in the electrolyte increased with an increase in CO_2 pressure (Fig. S3†).[44] The detailed calculation of the concentrations of carbon species and protons in 0.1 M $KHCO_3$ at various CO_2 partial pressures is shown in the experimental section of the ESI.†

The CO_2RR product distribution at ambient and high pressures (100 bar) is shown in Fig. 2b and c. A linear sweep voltammetry (LSV) test was conducted with a sweep rate of 20 mV s^{-1} at different CO_2 pressures. It should be noted that the LSV curves emerged with a decreasing trend of the overpotential and an increase in current density (Fig. 2d and Fig. S4†), suggesting the immense impact of the different CO_2 pressures in the CO_2RR. Product analysis at a low overpotential of 1 bar revealed that the reaction was dominant by the competitive HER (ranging from −1.2 V *vs.* Ag/AgCl to −1.6 V *vs.* Ag/AgCl, $FE_{H_2} > 60\%$) (Fig. 2b and Fig. S5†). Though the HER was suppressed at a high overpotential (ranging from −1.7 V *vs.* Ag/AgCl to −2.1 V *vs.* Ag/AgCl, $FE_{H_2} < 40\%$), a wide CO_2RR product distribution was observed. It could be seen that CO was the dominant C_1 product ($FE_{CO} = 25.7\%$ at −1.8 V *vs.* Ag/AgCl) and ethylene was the main C_{2+} product ($FE_{ethylene} = 27.8\%$ at −2.1
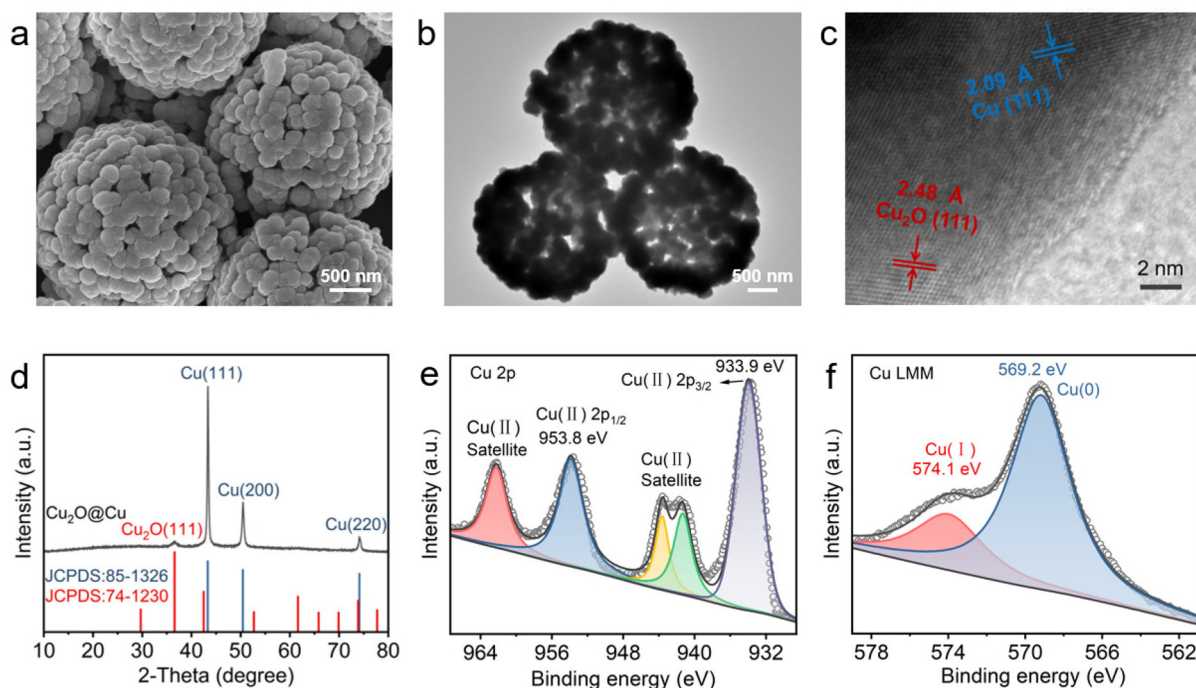
Fig. 1 Characterization of the as-prepared HS-Cu catalyst. (a) SEM image, (b and c) HRTEM image, (d) XRD pattern, (e and f) XPS Cu 2p and Cu LMM Auger electron spectra of $Cu_2O@Cu$.
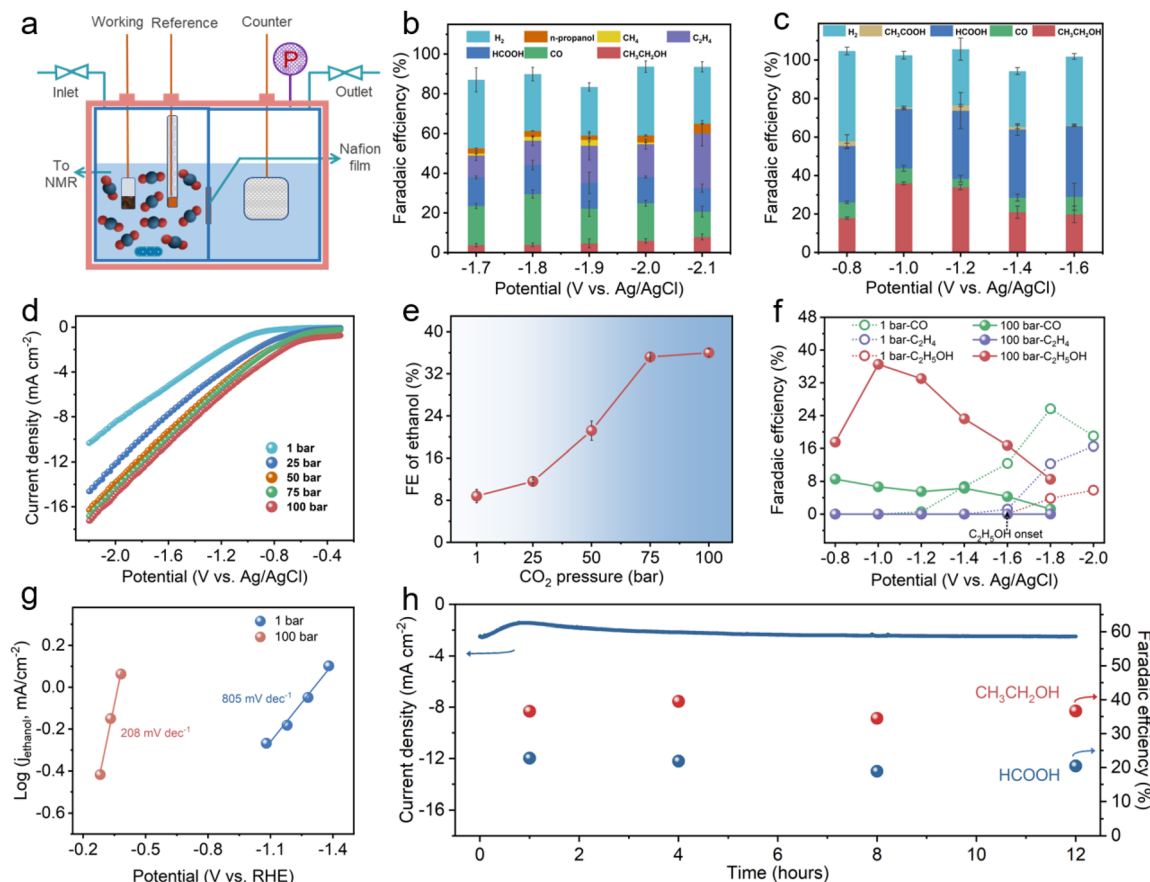
Fig. 2 CO_2RR performance at different CO_2 pressures. (a) Schematic description of the high-pressure electrolytic cell. (b) Faradaic efficiencies of different products on the HS-Cu electrode at 1 bar and various potentials for one hour test. (c) Faradaic efficiencies of different products on the HS-Cu electrode at 100 bar and various potentials. (d) LSV of HS-Cu in 0.1 M $KHCO_3$ aqueous solution at different CO_2 pressures. (e) Correlation of $FE_{ethanol}$ and CO_2 pressure. (f) A comparison of the potential-dependent FE_{CO}, $FE_{ethylene}$ and $FE_{ethanol}$ at 1 bar and 100 bar CO_2 pressure. (g) Tafel slopes for the ethanol partial current density ($j_{ethanol}$) at 1 and 100 bar. (h) Stability test of the HS-Cu catalyst on a glassy carbon electrode at 100 bar CO_2 pressures at a potential of −1.0 V *vs.* Ag/AgCl (non-iR corrected. The red and purple balls represent the corresponding FEs of ethanol and formate, respectively).

V *vs.* Ag/AgCl). In addition, the maximum $FE_{ethanol}$ was only 7.9% at −2.1 V *vs.* Ag/AgCl.

However, the product selectivity of the CO_2RR at different high pressures (25 bar, 50 bar, 75 bar and 100 bar) showed a significant difference. In particular, analysis of the liquid products illustrated that the selectivity of ethanol was obviously improved with increasing CO_2 pressure. The $FE_{ethanol}$ values at 25 bar, 50 bar and 75 bar were 11.8%, 22.8% and 35.8%, respectively (Fig. S6–S8†). Remarkably, a $FE_{ethanol}$ of 36.6% was achieved at a higher CO_2 pressure of 100 bar, which was 4.6 times higher than that obtained at 1 bar. Also, only −1.0 V *vs.* Ag/AgCl (−0.48 V *vs.* RHE) was required for the cathodic reduction, which is a low reduction overpotential for the CO_2RR to ethanol (Fig. 2c). To reveal the variation tendency of $FE_{ethanol}$ influenced by different high CO_2 pressures, the correlation between $FE_{ethanol}$ and CO_2 pressure was studied (Fig. 2e). The FE of ethanol was rapidly enhanced upon increasing the CO_2 pressure from 1 bar to 75 bar. When the pressure continued to rise to 100 bar, the $FE_{ethanol}$ reached a plateau. This indi-

cates that the $FE_{ethanol}$ is mainly affected by the CO_2 pressure up to supercritical CO_2 conditions. Surprisingly, a significant decrease in $FE_{ethylene}$ was observed accordingly. A very low $FE_{ethylene}$ of 3.5% was attained at 25 bar and no ethylene was detected at 50 bar, 75 bar and 100 bar as shown in Fig. 2c and Fig. S6–S8.† These results manifest that the ethylene product, as the competitive product of ethanol, was restrained by suppressing at the same potentials at 100 bar, which we surmise is due to the higher CO_2 solubility at the high pressure (Fig. 2c and Fig. S5†).[46,52,53] For C_1 products, as displayed in Fig. 2c and Fig. S5–S8,† FE_{CO} was decreased and FE_{HCOOH} was improved at a high CO_2 pressure. Moreover, FE_{CO}, $FE_{ethylene}$ and $FE_{ethanol}$ in the potential range of −0.8 to −2.0 V *vs.* Ag/AgCl at 1 bar and 100 bar are presented in Fig. 2f, which revealed a super-low ethanol overpotential (<−0.8 V *vs.* Ag/AgCl (<−0.3 V *vs.* RHE)) at 100 bar in contrast to that at 1 bar (−1.6 V *vs.* Ag/AgCl).[20] The $FE_{ethanol}$ was increased accompanied by the decrease of FE_{CO} at 100 bar, which strongly implies that CO is a vital intermediate for the CO_2RR to ethanol.

To investigate whether the product distribution is caused by CO_2 pressure directly or pH changes at high CO_2 pressure, the CO_2RR experiments at 1 bar used 0.1 M $KHCO_3$ + H_2SO_4 aqueous solutions of pH ∼ 5.0 as the electrolyte was operated. As shown in Fig. S10,† a similar product distribution was obtained in the CO_2RR at 1 bar in different local pH environments, which indicates that the $FE_{C_{2+}}$ switching with the increase of CO_2 pressure is due to the CO_2 pressure inherently. For the CORR of the HS-Cu catalyst, a similar trend for $FE_{ethylene}$ has been observed in the CORR at different CO pressures shown in Fig. S11,† which indicated that $FE_{ethylene}$ was decreased with the CO concentration increase. There is no noticeable change in $FE_{ethanol}$ at 1 bar and 3 bar, which is probably due to the other C_{2+} competitive products.

In order to compare the reaction kinetics of the CO_2RR at ambient and high pressures, we obtained Tafel slopes for the CO_2RR current density attributed to ethanol production ($j_{ethanol}$). The slopes were found to be 208 mV dec^{-1} and 805 mV dec^{-1} for 100 bar and 1 bar, respectively (Fig. 2g). The decreased Tafel slope value with increased CO_2 pressure suggested that a faster reaction kinetics could be achieved at a higher CO_2 pressure.[44] In addition, the continuous CO_2RR at 100 bar was performed at −1.0 V vs. Ag/AgCl for 12 h to illuminate the long-term stability of the HS-Cu. As displayed in Fig. 2h, there were no obvious changes in both the current density and FE of the ethanol and formate, illustrating the excellent stability of the prepared HS-Cu catalyst at a high CO_2 pressure.[52] Furthermore, XRD, XPS and SEM of the electrode after the CO_2RR at 100 bar were characterized. Only characteristic peaks of bare Cu could be observed from the XRD pattern (Fig. S12†), but a minor signal of the Cu^+ peak was detected from XPS analysis (Fig. S13†), which could be ascribed to the reoxidation of Cu^0 after exposure to air during the sample transfer process. The SEM image showed that the sample still exhibited the hollow sphere morphology (Fig. S14†), which further indicated the good stability of the catalyst.

To gain insight into the reaction mechanism on HS-Cu for the CO_2RR at different CO_2 pressures, in situ Raman measurement was conducted at various applied potentials in a custommade high pressure in situ Raman cell (Fig. S15†). As shown in Fig. 3 and Fig. S16,† the spectra at different potentials were collected to uncover the reaction intermediates at different CO_2 pressures. The C≡O stretching vibration of adsorbed *CO at ca. 2091 cm^{-1} and the C–H stretching vibration of adsorbed CH_3 at ca. 2861 and 2930 cm^{-1} were clearly observed at negative applied potentials from −0.8 V to −1.3 V vs. Ag/AgCl at 80 bar (Fig. 3a), which could be assigned to the key intermediates for producing ethanol.[57–59] Moreover, the peaks at ca. 278 cm^{-1} and 352 cm^{-1} assigned to the Cu–CO stretching vibration modes could be unambiguously detected. In addition, a broad peak emerging at ca. 2091 cm^{-1} corresponds to the *CO vibrational mode. With the applied potential being increased to −1.3 V vs. Ag/AgCl, the peak intensity increased continuously, which indicates that the *CO coverage on the catalyst was improved (Fig. 3a).[60] Furthermore, in situ Raman spectra at different CO_2 pressures were compared at a controlled potential (−1.0 V vs. Ag/AgCl). Due to the weak adsorption of *CO on the catalyst surface at ambient pressure, no obvious peak could be observed at different potentials at 1 bar CO_2 pressure. The elevated peak intensity of the Cu–CO and *CO stretching vibrations with the increased CO_2 pressure from 1 bar to 80 bar is due to the effective enrichment of the adsorbed *CO intermediates on the surface of the catalyst under the high-pressure conditions (Fig. 3b). In situ Raman data collected at various applied potentials and CO_2 pressures thus directly and clearly demonstrates that the high CO_2 pressure contributes to improving the *CO coverage on the catalyst,[60,61] which effectively promotes C–C coupling and enhances ethanol selectivity. Besides, the characteristic Cu_2O peaks at around 520 cm^{-1} and 620 cm^{-1} disappeared with the overpotential from −0.1 to −1.3 V vs. Ag/AgCl, further indicating that only Cu(0) existed stably during the CO_2RR at high pressure (Fig. S16†).
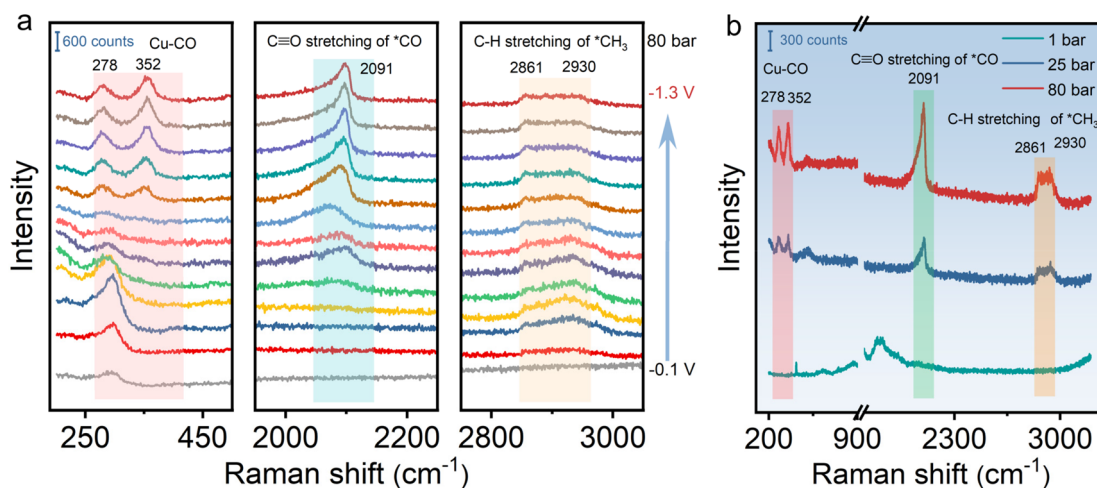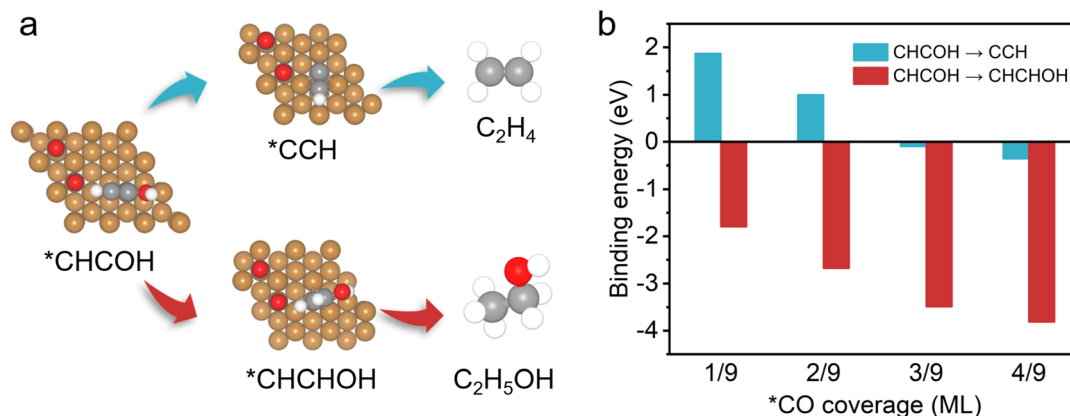

Fig. 3 In situ Raman spectra of HS-Cu obtained (a) in the potential range of −0.1 to −1.3 V vs. Ag/AgCl during the CO_2RR at 80 bar CO_2 pressure, (b) at different CO_2 pressures during the CO_2RR at a controlled potential of −1.0 V vs. Ag/AgCl.

Fig. 4 DFT calculation results on the effects of *CO coverage. (a) Key reaction pathways for the CO_2RR to ethylene and ethanol on the Cu(111) surface. Yellow, copper; grey, carbon; red, oxygen; and white, hydrogen. (b) Binding energies of *CCH (cyan) and *CHCHOH (red) intermediates at different *CO coverages on the Cu(111) surface.

On the basis of the observed pressure-dependent activity for CO_2 conversion to ethanol, DFT calculations were further conducted to gain a more in-depth understanding of the underlying relationship between the production pathways of ethylene, ethanol and the local *CO concentration on the catalyst surface (Fig. 4 and S17†). Previous reports proposed that the formation of the intermediate *CHCOH is a decisive step in generating C_{2+} products during the process of the CO_2RR on the Cu(111) surface model systems.[60,62] The *CHCOH intermediate is further hydrogenated to form *CCH and *CHCHOH, which are the critical intermediates for ethylene and ethanol formation, respectively (Fig. 4a). We first calculated the binding energy of *CHCHOH and *CCH intermediates (Fig. 4b). We found that the binding energy decreases more for the formation of *CHCHOH (ethanol path) compared with that of *CCH (ethylene path) in the presence of *CO. With the increase of *CO coverage from 1/9–4/9 ML, the binding energy of *CHCHOH intermediates also reduces continuously, which indicates that more heat is released during the formation of *CHCHOH intermediates. Therefore, we discovered that higher *CO coverage on the catalyst surface effectively facilitates the selective formation of ethanol rather than ethylene. Besides, it is reasonable to calculate the required free energy for generating the intermediates *CCH and *CHCHOH to evaluate the possible reaction paths (Fig. S18†). The free energy of *CHCHOH decreases more than that of *CCH with *CO coverage reaching from 1/9 to 4/9. This phenomenon, which allows for high *CO coverage on the catalyst surface, is beneficial for generating *CHCHOH, thus promoting the production of ethanol. The good agreement with experimental results and the DFT calculations suggests that the selectivity for C_{2+} products in the CO_2RR could be effectively controlled by modulating the *CO coverage on the surface of Cu-based catalysts.

Furthermore, we have also conducted techno-economic analysis (TEA) of the electrocatalytic CO_2 conversion to ethanol at high pressures. From the technology and its impact on society, the process of electrochemical CO_2 reduction to produce ethanol is the green pathway for CO_2 conversion relevant to carbon reduction/utilization. Meanwhile, the high-pressure strategy does not obviously depend on the pressurization/CO_2 supply cost but mainly on the electrolysis energy cost (as displayed in the ESI† in detail).

Conclusions

In summary, different CO_2 pressures from 1 to 100 bar were facilely introduced into an electrochemical CO_2RR system to regulate the product selectivity, and it was interesting to find that the main C_{2+} products could be switched from ethylene at ambient pressure to ethanol under high pressure conditions over the HS-Cu catalyst. In our work, the $FE_{ethanol}$ could reach as high as 36.6% at 100 bar CO_2 pressure, which is 4.6 times higher than that of 1 bar accompanied by faster kinetics and lower overpotential for ethanol formation. *In situ* Raman spectra at different pressures prove that higher *CO coverage on the surface of the HS-Cu catalyst could be detected at higher CO_2 pressures. DFT calculations further confirmed that higher *CO coverage at a high CO_2 pressure on the Cu surface effectively facilitates the selective formation of ethanol rather than ethylene. This work provides a facile strategy for regulating CO_2 conversion into ethanol by using renewable electricity with the assistance of high CO_2 pressure. In particular, to further enhance the $FE_{ethanol}$, the CO_2RR performance of other Cu-based catalysts which have already been demonstrated with good $FE_{ethylene}$ or $FE_{ethanol}$ under ambient conditions will be evaluated with the assistance of high CO_2 pressures in the near future. Moreover, we believe that the interesting observation under a high pressure CO_2 regulation system reported here could also be extended to plenty of other novel catalysts for the efficient conversion of CO_2 to high value-added chemicals and fuels.

Author contributions

R. X. Q., L. P., S. L. Y., and J. L. proposed the project, designed the experiments, and wrote the manuscript. R. X. Q. performed the whole experiment. J. J., and Y. Z. G. conducted the DFT calculations. J. R. L., J. Z., D. T. S., Z. Y. L., and C. L. performed the analysis of experimental data. R. Q. L., S. Y., and B. R. conducted a part of the characterization studies. Z. P. L., T. W. X., G. K. X., L. X. C., and Y. Z. H. participated in the discussions. L. P., S. L. Y., J. L., and B. X. H. supervised the whole project.

Conflicts of interest

There are no conflicts to declare.

Acknowledgements

Notes and references

1 R. Dawson, E. Stöckel, J. R. Holst, D. J. Adams and A. I. Cooper, *Energy Environ. Sci.*, 2011, **4**, 4239–4245.

2 G. Wang, J. Chen, Y. Ding, P. Cai, L. Yi, Y. Li, C. Tu, Y. Hou, Z. Wen and L. Dai, *Chem. Soc. Rev.*, 2021, **50**, 4993–5061.

3 G. Wen, B. Ren, Y. Zheng, M. Li, C. Silva, S. Song, Z. Zhang, H. Dou, L. Zhao, D. Luo, A. Yu and Z. Chen, *Adv. Energy Mater.*, 2021, **12**, 2103289.

4 R. G. Mariano, K. McKelvey, H. S. White and M. W. Kanan, *Science*, 2017, **358**, 1187–1192.

5 W. Guo, X. Tan, J. Bi, L. Xu, D. Yang, C. Chen, Q. Zhu, J. Ma, A. Tayal, J. Ma, Y. Huang, X. Sun, S. Liu and B. Han, *J. Am. Chem. Soc.*, 2021, **143**, 6877–6885.

6 L. Jiao, W. Yang, G. Wan, R. Zhang, X. Zheng, H. Zhou, S. H. Yu and H. L. Jiang, *Angew. Chem., Int. Ed.*, 2020, **59**, 20589–20595.

7 X. Suo, F. Zhang, Z. Yang, H. Chen, T. Wang, Z. Wang, T. Kobayashi, C. L. Do-Thanh, D. Maltsev, Z. Liu and S. Dai, *Angew. Chem., Int. Ed.*, 2021, **60**, 25688–25694.

8 T. Zheng, C. Liu, C. Guo, M. Zhang, X. Li, Q. Jiang, W. Xue, H. Li, A. Li, C. W. Pao, J. Xiao, C. Xia and J. Zeng, *Nat. Nanotechnol.*, 2021, **16**, 1386–1393.

9 Z. Wang, Y. Zhou, D. Liu, R. Qi, C. Xia, M. Li, B. You and B. Y. Xia, *Angew. Chem., Int. Ed.*, 2022, **61**, e202200552.

10 D. L. Meng, M. D. Zhang, D. H. Si, M. J. Mao, Y. Hou, Y. B. Huang and R. Cao, *Angew. Chem., Int. Ed.*, 2021, **60**, 25485–25492.

11 X. F. Qiu, H. L. Zhu, J. R. Huang, P. Q. Liao and X. M. Chen, *J. Am. Chem. Soc.*, 2021, **143**, 7242–7246.

12 P. Shao, W. Zhou, Q. L. Hong, L. Yi, L. Zheng, W. Wang, H. X. Zhang, H. Zhang and J. Zhang, *Angew. Chem., Int. Ed.*, 2021, **60**, 16687–16692.

13 D. Wakerley, S. Lamaison, F. Ozanam, N. Menguy, D. Mercier, P. Marcus, M. Fontecave and V. Mougel, *Nat. Mater.*, 2019, **18**, 1222–1227.

14 C. Chen, X. Yan, S. Liu, Y. Wu, Q. Wan, X. Sun, Q. Zhu, H. Liu, J. Ma, L. Zheng, H. Wu and B. Han, *Angew. Chem., Int. Ed.*, 2020, **59**, 16459–16464.

15 X. Wang, Z. Wang, F. P. García de Arquer, C.-T. Dinh, A. Ozden, Y. C. Li, D.-H. Nam, J. Li, Y.-S. Liu, J. Wicks, Z. Chen, M. Chi, B. Chen, Y. Wang, J. Tam, J. Y. Howe, A. Proppe, P. Todorović, F. Li, T.-T. Zhuang, C. M. Gabardo, A. R. Kirmani, C. McCallum, S.-F. Hung, Y. Lum, M. Luo, Y. Min, A. Xu, C. P. O'Brien, B. Stephen, B. Sun, A. H. Ip, L. J. Richter, S. O. Kelley, D. Sinton and E. H. Sargent, *Nat. Energy*, 2020, **5**, 478–486.

16 H. Xu, D. Rebollar, H. He, L. Chong, Y. Liu, C. Liu, C.-J. Sun, T. Li, J. V. Muntean, R. E. Winans, D.-J. Liu and T. Xu, *Nat. Energy*, 2020, **5**, 623–632.

17 X. Su, Z. Jiang, J. Zhou, H. Liu, D. Zhou, H. Shang, X. Ni, Z. Peng, F. Yang, W. Chen, Z. Qi, D. Wang and Y. Wang, *Nat. Commun.*, 2022, **13**, 1322.

18 H. Han, Y. Noh, Y. Kim, S. Park, W. Yoon, D. Jang, S. M. Choi and W. B. Kim, *Green Chem.*, 2020, **22**, 71–84.

19 C. Peng, G. Luo, J. Zhang, M. Chen, Z. Wang, T. K. Sham, L. Zhang, Y. Li and G. Zheng, *Nat. Commun.*, 2021, **12**, 1580.

20 D. Ren, N. T. Wong, A. D. Handoko, Y. Huang and B. S. Yeo, *J. Phys. Chem. Lett.*, 2016, **7**, 20–24.

21 D. Karapinar, C. E. Creissen, J. G. Rivera de la Cruz, M. W. Schreiber and M. Fontecave, *ACS Energy Lett.*, 2021, **6**, 694–706.

22 J. Santatiwongchai, K. Faungnawakij and P. Hirunsit, *ACS Catal.*, 2021, **11**, 9688–9701.

23 S. Nitopi, E. Bertheussen, S. B. Scott, X. Liu, A. K. Engstfeld, S. Horch, B. Seger, I. E. L. Stephens, K. Chan, C. Hahn, J. K. Norskov, T. F. Jaramillo and I. Chorkendorff, *Chem. Rev.*, 2019, **119**, 7610–7672.

24 W. Ma, X. He, W. Wang, S. Xie, Q. Zhang and Y. Wang, *Chem. Soc. Rev.*, 2021, **50**, 12897–12914.

25 C. Kim, K. M. Cho, K. Park, J. Y. Kim, G. T. Yun, F. M. Toma, I. Gereige and H. T. Jung, *Adv. Funct. Mater.*, 2021, **31**, 2102142.

26 J. Wang, H. Y. Tan, Y. Zhu, H. Chu and H. M. Chen, *Angew. Chem., Int. Ed.*, 2021, **60**, 17254–17267.

27 Q. Zhu, X. Sun, D. Yang, J. Ma, X. Kang, L. Zheng, J. Zhang, Z. Wu and B. Han, *Nat. Commun.*, 2019, **10**, 3851.

28 Z. Chen, T. Wang, B. Liu, D. Cheng, C. Hu, G. Zhang, W. Zhu, H. Wang, Z. J. Zhao and J. Gong, *J. Am. Chem. Soc.*, 2020, **142**, 6878–6883.

29 O. Piqué, F. Viñes, F. Illas and F. Calle-Vallejo, *ACS Catal.*, 2020, **10**, 10488–10494.

30 C. Zhu, Z. Zhang, L. Zhong, C.-S. Hsu, X. Xu, Y. Li, S. Zhao, S. Chen, J. Yu, S. Chen, M. Wu, P. Gao, S. Li, H. M. Chen, K. Liu and L. Zhang, *Chem*, 2021, **7**, 406–420.

31 J. J. Lv, M. Jouny, W. Luc, W. Zhu, J. J. Zhu and F. Jiao, *Adv. Mater.*, 2018, **30**, e1803111.

32 X. Feng, K. Jiang, S. Fan and M. W. Kanan, *ACS Cent. Sci.*, 2016, **2**, 169–174.

33 A. N. Kuhn, H. Zhao, U. O. Nwabara, X. Lu, M. Liu, Y. T. Pan, W. Zhu, P. J. A. Kenis and H. Yang, *Adv. Funct. Mater.*, 2021, **31**, 2101668.

34 Y. Zhou, F. Che, M. Liu, C. Zou, Z. Liang, P. De Luna, H. Yuan, J. Li, Z. Wang, H. Xie, H. Li, P. Chen, E. Bladt, R. Quintero-Bermudez, T. K. Sham, S. Bals, J. Hofkens, D. Sinton, G. Chen and E. H. Sargent, *Nat. Chem.*, 2018, **10**, 974–980.

35 R. Feng, Q. Zhu, M. Chu, S. Jia, J. Zhai, H. Wu, P. Wu and B. Han, *Green Chem.*, 2020, **22**, 7560–7565.

36 Y. Wang, P. Han, X. Lv, L. Zhang and G. Zheng, *Joule*, 2018, **2**, 2551–2582.

37 Z. Z. Niu, F. Y. Gao, X. L. Zhang, P. P. Yang, R. Liu, L. P. Chi, Z. Z. Wu, S. Qin, X. Yu and M. R. Gao, *J. Am. Chem. Soc.*, 2021, **143**, 8011–8021.

38 S. Jia, Q. Zhu, M. Chu, S. Han, R. Feng, J. Zhai, W. Xia, M. He, H. Wu and B. Han, *Angew. Chem., Int. Ed.*, 2021, **60**, 10977–10982.

39 J. Huang, M. Mensi, E. Oveisi, V. Mantella and R. Buonsanti, *J. Am. Chem. Soc.*, 2019, **141**, 2490–2499.

40 Y. Liu, Y. Zhang, K. Cheng, X. Quan, X. Fan, Y. Su, S. Chen, H. Zhao, Y. Zhang, H. Yu and M. R. Hoffmann, *Angew. Chem., Int. Ed.*, 2017, **56**, 15607–15611.

41 Y. Song, W. Chen, C. Zhao, S. Li, W. Wei and Y. Sun, *Angew. Chem., Int. Ed.*, 2017, **56**, 10840–10844.

42 N. Sikdar, J. R. C. Junqueira, S. Dieckhöfer, T. Quast, M. Braun, Y. Song, H. B. Aiyappa, S. Seisel, J. Weidner, D. Ohl, C. Andronescu and W. Schuhmann, *Angew. Chem., Int. Ed.*, 2021, **60**, 23427–23434.

43 S. Kaneco, N.-h. Hiei, Y. Xing, H. Katsumata, H. Ohnishi, T. Suzuki and K. Ohta, *J. Solid State Electrochem.*, 2003, **7**, 152–156.

44 C. M. Gabardo, A. Seifitokaldani, J. P. Edwards, C.-T. Dinh, T. Burdyny, M. G. Kibria, C. P. O'Brien, E. H. Sargent and D. Sinton, *Energy Environ. Sci.*, 2018, **11**, 2531–2539.

45 C. I. Shaughnessy, D. J. Sconyers, H.-J. Lee, B. Subramaniam, J. D. Blakemore and K. C. Leonard, *Green Chem.*, 2020, **22**, 2434–2442.

46 J. Li, Y. Kuang, Y. Meng, X. Tian, W. H. Hung, X. Zhang, A. Li, M. Xu, W. Zhou, C. S. Ku, C. Y. Chiang, G. Zhu, J. Guo, X. Sun and H. Dai, *J. Am. Chem. Soc.*, 2020, **142**, 7276–7282.

47 J. Li, J. Guo and H. Dai, *Sci. Adv.*, 2022, **8**, eabo0399.

48 M. Asadi, K. Kim, C. Liu, A. V. Addepalli, P. Abbasi, P. Yasaei, P. Phillips, A. Behranginia, J. M. Cerrato, R. Haasch, P. Zapol, B. Kumar, R. F. Klie, J. Abiade, L. A. Curtiss and A. Salehi-Khojin, *Science*, 2016, **353**, 467–470.

49 X. Kang, L. Li, A. Sheveleva, X. Han, J. Li, L. Liu, F. Tuna, E. J. L. McInnes, B. Han, S. Yang and M. Schroder, *Nat. Commun.*, 2020, **11**, 5464.

50 D. V. Vasilyev and P. J. Dyson, *ACS Catal.*, 2021, **11**, 1392–1405.

51 C. I. Shaughnessy, D. J. Sconyers, T. A. Kerr, H. J. Lee, B. Subramaniam, K. C. Leonard and J. D. Blakemore, *ChemSusChem*, 2019, **12**, 3761–3768.

52 K. j. Puring, O. Evers, M. Prokein, D. Siegmund, F. Scholten, N. Mölders, M. Renner, B. Roldan Cuenya, M. Petermann, E. Weidner and U.-P. Apfel, *ACS Catal.*, 2020, **10**, 12783–12789.

53 S. Lamaison, D. Wakerley, J. Blanchard, D. Montero, G. Rousse, D. Mercier, P. Marcus, D. Taverna, D. Giaume, V. Mougel and M. Fontecave, *Joule*, 2020, **4**, 395–406.

54 J. Kou, A. Saha, C. Bennett-Stamper and R. S. Varma, *Chem. Commun.*, 2012, **48**, 5862–5864.

55 T. C. Chou, C. C. Chang, H. L. Yu, W. Y. Yu, C. L. Dong, J. J. Velasco-Velez, C. H. Chuang, L. C. Chen, J. F. Lee, J. M. Chen and H. L. Wu, *J. Am. Chem. Soc.*, 2020, **142**, 2857–2867.

56 M. Li, Y. Ma, J. Chen, R. Lawrence, W. Luo, M. Sacchi, W. Jiang and J. Yang, *Angew. Chem., Int. Ed.*, 2021, **60**, 11487–11493.

57 D. Ren, J. Gao, L. Pan, Z. Wang, J. Luo, S. M. Zakeeruddin, A. Hagfeldt and M. Gratzel, *Angew. Chem., Int. Ed.*, 2019, **58**, 15036–15040.

58 F. Hu, L. Yang, Y. Jiang, C. Duan, X. Wang, L. Zeng, X. Lv, D. Duan, Q. Liu, T. Kong, J. Jiang, R. Long and Y. Xiong, *Angew. Chem., Int. Ed.*, 2021, **60**, 26122–26127.

59 A. D. Handoko, K. W. Chan and B. S. Yeo, *ACS Energy Lett.*, 2017, **2**, 2103–2109.

60 F. Li, Y. C. Li, Z. Wang, J. Li, D.-H. Nam, Y. Lum, M. Luo, X. Wang, A. Ozden, S.-F. Hung, B. Chen, Y. Wang, J. Wicks, Y. Xu, Y. Li, C. M. Gabardo, C.-T. Dinh, Y. Wang, T.-T. Zhuang, D. Sinton and E. H. Sargent, *Nat. Catal.*, 2019, **3**, 75–82.

61 Z. Gu, H. Shen, Z. Chen, Y. Yang, C. Yang, Y. Ji, Y. Wang, C. Zhu, J. Liu, J. Li, T.-K. Sham, X. Xu and G. Zheng, *Joule*, 2021, **5**, 429–440.

62 Y. W. Lum, T. Cheng, W. A. Goddard and J. W. Ager, *J. Am. Chem. Soc.*, 2018, **140**, 9337–9340.